Supporting Information II: Supplemental Experimental Data

Analysis of multi-electron, multi-step homogeneous catalysis by rotating disc electrode voltammetry: Theory, application, and obstacles

Katherine J. Lee,† Cole T. Gruninger,† Kunal M. Lodaya,† Saad Qadeer,‡ Boyce E. Griffith,‡ and Jillian L. Dempsey†

†Department of Chemistry, University of North Carolina at Chapel Hill, Chapel Hill, North Carolina, USA 27599

‡Department of Mathematics, University of North Carolina at Chapel Hill, Chapel Hill, North Carolina, USA 27599

Table of Contents *Page*

Glossary of Symbols

A: geometric electrode surface area (cm^2)

C_A^0: bulk concentration of acid

C_P^0: bulk concentration of catalyst

$D_{species}$: diffusion coefficient of the subscript species ($cm^2\ s^{-1}$)

E: potential (V)

$E^{0\prime}$: formal potential of the reduction process (V)

E_n: formal potential for the nth electron transfer in a catalytic cycle (V)

ΔE: potential difference between E_2 and E_1 (V), $\Delta E = E_2 - E_1$

F: Faraday's constant

f: F/RT (V^{-1})

i_c: observed catalytic current (A)

i_p: diffusion-controlled plateau current of the catalyst (A)

i_{peak}: diffusion-controlled peak current of the catalyst (A)

i_{pl}: plateau current (A)

k: rate constant for a chemical step

k_{FOWA}: observed rate constant extracted using FOWA

k_s: standard heterogeneous electrochemical rate constant ($cm\ s^{-1}$)

n: number of electrons transferred at the electrode in the redox event

R: gas constant

T: temperature (K)

α: transfer coefficient

θ: dimensionless potential scale, $\theta = -(f)\left(E - E_{couple}^{0\prime}\right)$

ν: kinematic viscosity ($cm\ s^{-1}$)

Ψ^{∞}: dimensionless plateau current, $\Psi^{\infty} = i_{pl}/i_p$

ω: rotation rate ($rad\ s^{-1}$)

SI-1 Determination of Diffusion Coefficient via RDEV and Comparison to Stationary Methods

The diffusion coefficient of $Co(dmgBF_2)_2(CH_3CN)_2$ was determined using rotation rate dependence studies between 42 and 262 rad s^{-1}. Data collected at 377 rad s^{-1} and above showed deviations from the idealized sigmoidal waveform, indicative of a kinetic limitation imposed by electron transfer, and thus was not included in this analysis.

The plateau current linearly correlates with $\omega^{1/2}$ as predicted via the Levich equation which relates the plateau current of a reversible, diffusion controlled redox process to ω (eq. S1).[1] The Levich equation was used to calculate a diffusion coefficient of 9.15 x 10^{-6} cm^2 s^{-1}. This value is in excellent agreement with the diffusion coefficient obtained using stationary voltammetry (D = 9.22 x 10^{-6} cm^2 s^{-1}) and electrochemical simulation (D = 8 x 10^{-6} cm^2 s^{-1}).[2,3]

$$i_p = 0.620nFAD^{2/3}\nu^{-1/6}\omega^{1/2}C_P^0 \qquad \text{(eq. S1)}$$

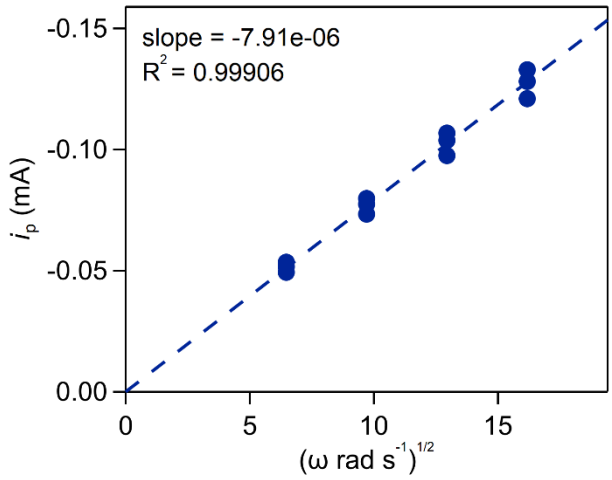

Figure S1 The cathodic limiting current of the $Co^{II/I}$ couple as a function of $\omega^{1/2}$. The slope of this line corresponds to $0.620nFAD^{2/3}\nu^{-1/6}C_P^0$ per the Levich equation and can be used to extract the diffusion coefficient. Experimental data indicated by blue dots. Dashed line represents the linear fit.

SI-2 Effects of Acid Identity, Concentration, and Rotation Rate on Catalytic Voltammograms

Extracting figures of merit from catalytic voltammograms

For RDE voltammograms with inclined plateau currents that did not reach a limiting current value, two metrics were considered as estimates of the plateau current. (Note: In cases where an exponential current rise could be easily identified near the vertex potential – see red trace in **Figure S4** as an example – only current values in the non-curved region were considered for both approximation methodologies.) The first used the maximum current reached in the sloping plateau as an estimate of plateau current. The second used the base coefficient determined by the sigmoidal curve fitting function in Igor Pro 7.08. While both methods are expected to introduce quantitative error into the measurement, they produce plateau currents that show qualitatively similar behavior. As such, both metrics were considered accurate enough to allow qualitative trends to be identified. In this work, for current-potential responses with inclined plateaus, the catalytic plateau current was approximated as the maximum measured current. Voltammograms of 0.5 mM $Co(dmgBF_2)_2(CH_3CN)_2$ with 5 mM 4-methoxyanilinium are provided as an example data sets to illustrate the two approximation methods. These voltammograms were collected in the same solution with the same electrode, which was not re-polished between scans. Voltammograms were recorded at rotation rates spanning 42 – 262 rad sec^{-1}, which were employed in ascending order.

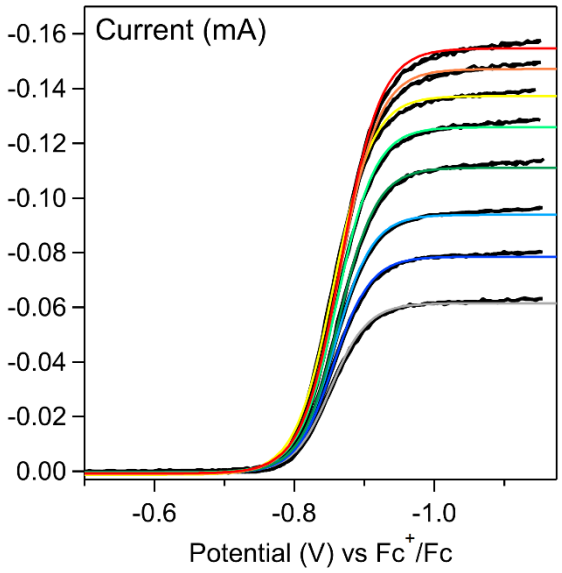

Figure S2 RDE voltammograms of 0.5 mM $Co(dmgBF_2)_2(CH_3CN)_2$ with 5 mM 4-methoxyanilinium at different rotation rates. Experimental data (black) overlaid with corresponding sigmoidal fits for voltammograms collected at 42 (grey), 68 (dark blue), 94 (light blue), 131 (dark green), 168 (light green), 199 (yellow), 230 (orange), and 262 (red) rad sec^{-1}. Voltammograms recorded in 0.25 M $[NBu_4][PF_6]$ acetonitrile at 0.01 V sec^{-1}.

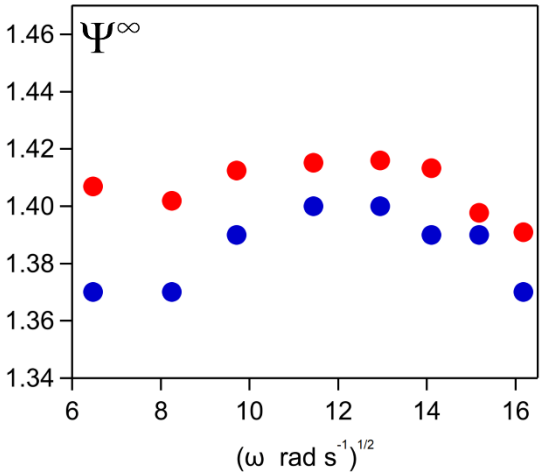

Figure S3 Comparison of estimated Ψ^{∞} value for 0.5 mM $Co(dmgBF_2)_2(CH_3CN)_2$ with 5 mM 4-methoxyanilinium when i_{pl} is extracted from sigmoidal fitting (blue) or the maximum current observed in the plateau region (red). While slight quantitative differences can be observed between the two metrics, similar qualitative behavior is observed.

Plateau currents as a function of acid concentration

Catalytic plateau currents will linearly depend on [acid]$^{1/2}$ for reactions that are first order in acid when the current-potential response is governed by the kinetics of the catalytic reaction. In contrast, a first-order dependence of the plateau current on [acid] will be observed when the plateau current is governed by the diffusion of substrate into the reaction layer.[4] In stationary electrochemical studies, a half-order dependence was observed for weaker acids (pK_a ≥ 9.7) while a linear dependence with a slope of -0.3 mA cm^{-2} M^{-1} was observed for stronger acids (pK_a ≤ 9.28).[2]

The relationship between plateau current and acid concentration was evaluated for RDE voltammograms of 4-trifluoromethoxyanilinium and anilinium. All voltammograms were collected at 42 rad sec^{-1}. For anilinium (pK_a = 10.62), plots of plateau current vs. [acid]$^{1/2}$ are linear. In contrast, for 4-trifluoromethoxyanilinium (pK_a = 9.28), a linear dependence is observed between the current density and [acid] with a slope of -0.3 mA cm^{-2} M^{-1}. Both data sets are consistent with results from stationary CV.

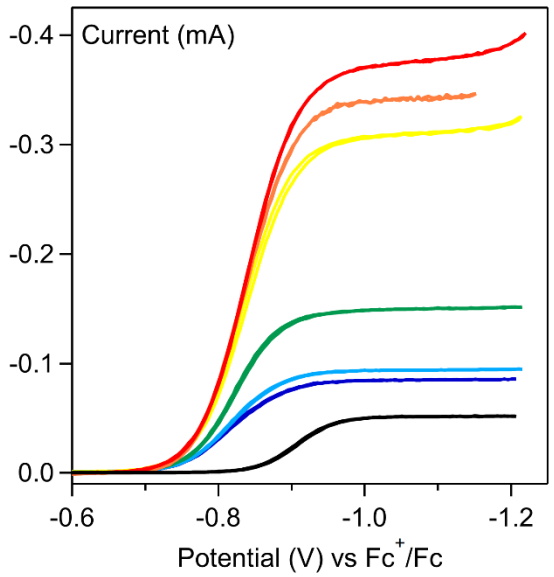

Figure S4 RDE voltammograms of 0.5 mM Co(dmgBF$_2$)(CH$_3$CN)$_2$ with 0 (black), 0.5 (blue), 0.55 (light blue), 1 (green), 4 (yellow), 5 (orange), and 5.5 (red) mM 4-trifluoromethoxyanilinium. Voltammograms recorded in 0.25 M [NBu$_4$][PF$_6$] acetonitrile at 0.01 V sec^{-1}.

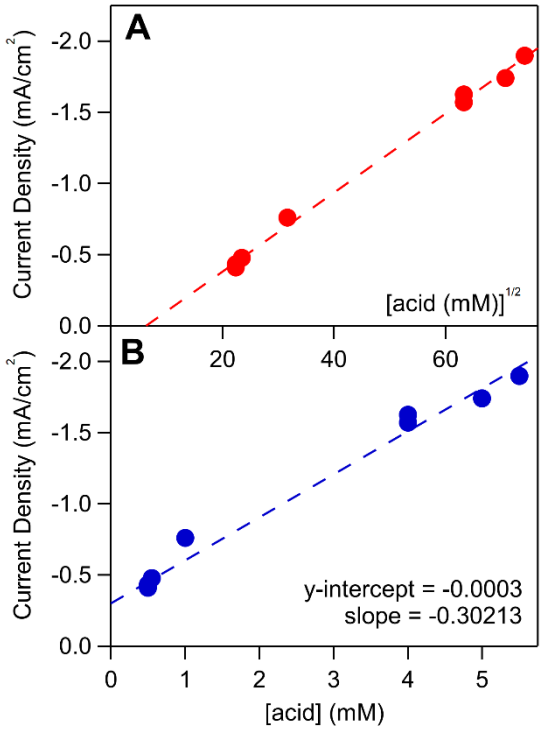

Figure S5 Current density as a function of (**A**) $[acid]^{1/2}$ and (**B**) [acid] for 4-trifluoromethoxyanilinium. In contrast to the current-$[acid]^{1/2}$ plot, the current-[acid] plot intercepts the y-axis at the current density value observed for $Co^{II/I}$ couple of $Co(dmgBF_2)_2(CH_3CN)_2$ in the absence of substrate.

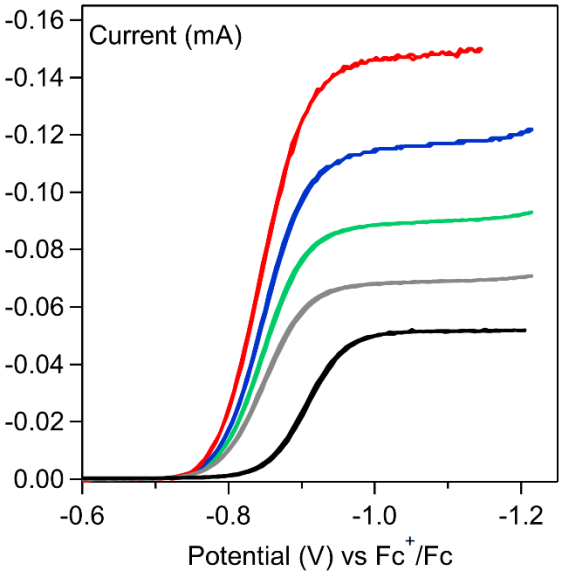

Figure S6 RDE voltammograms of 0.5 mM $Co(dmgBF_2)_2(CH_3CN)_2$ with 0 (black), 0.5 (grey), 1 (green), 2 (blue), and 5 (red) mM anilinium recorded in 0.25 M $[NBu_4][PF_6]$ acetonitrile at 0.01 V s^{-1}.

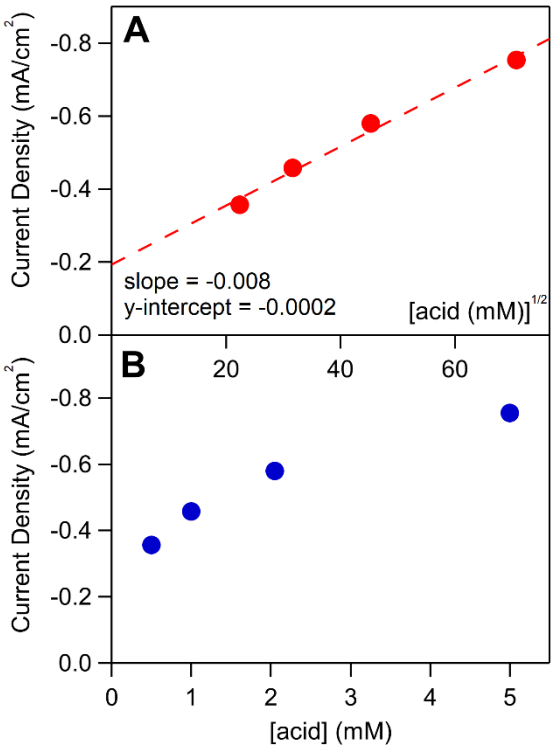

Figure S7 Current density as a function of (**A**) $[acid]^{1/2}$ and (**B**) [acid] for anilinium. A half-order dependence of plateau current on acid concentration is observed, indicating that the catalytic current response is not governed by diffusion of substrate into the reaction layer.

Catalytic voltammograms for variable rotation rate studies

Catalytic voltammograms were recorded for 0.5 mM $Co(dmgBF_2)_2(CH_3CN)_2$ in the presence of 1 or 10 equivalents 4-trifluoromethoxyanilinium, anilinium, and 4-methoxyanilinium at rotation rates ranging from 42-262 rad sec^{-1}. Trials for a given acid identity and concentration were collected using the same working electrode and solution such that a freshly prepared solution and pretreated working electrode were used for the first scan in a data set, but the solution and electrode were not refreshed in between voltammograms. For each set of trials, rotation rates were varied in ascending order (lowest to highest rotation rate). Voltammograms have not been baseline corrected to account for the increase in $i_{baseline}$ due to the accumulation of redox active products in the bulk solution (see section 3.3.1).

4-methoxyanilinium (pK_a = 11.86)

RDE voltammograms for variable rotation rate trials with 0.5 mM $Co(dmgBF_2)_2(CH_3CN)_2$ in the presence of 5 mM 4-methoxyanilinium shown in **Figure S2**.

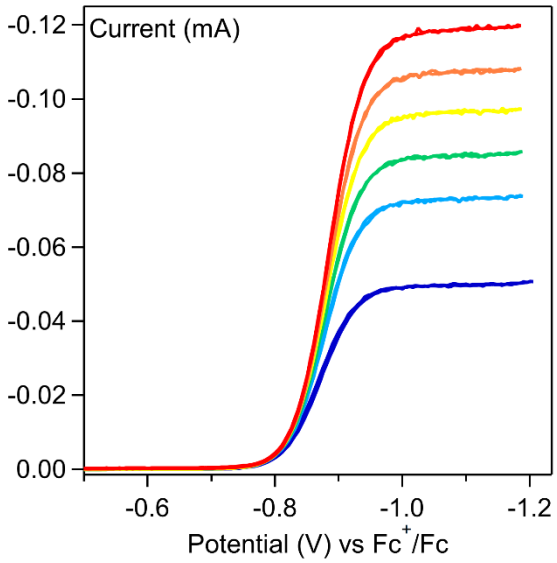

Figure S8 RDE voltammograms of 0.5 mM $Co(dmgBF_2)_2(CH_3CN)_2$ in the presence of 0.5 mM 4-methoxyanilinium at rotation rates of 42 (dark blue), 94 (light blue), 128 (green), 168 (yellow), 212 (orange), and 262 rad sec^{-1} (red). Voltammograms recorded at 0.01 V s^{-1} in 0.25 M $[NBu_4][PF_6]$ acetonitrile using a ferrocene (0.25 mM) internal standard. To reference voltammograms while avoiding the accumulation of ferrocenium in solution, stationary voltammograms were collected between RDE trials which scanned through the ferrocene redox couple. No major deviations in baseline current were observed.

Anilinium (pK_a = 10.62)

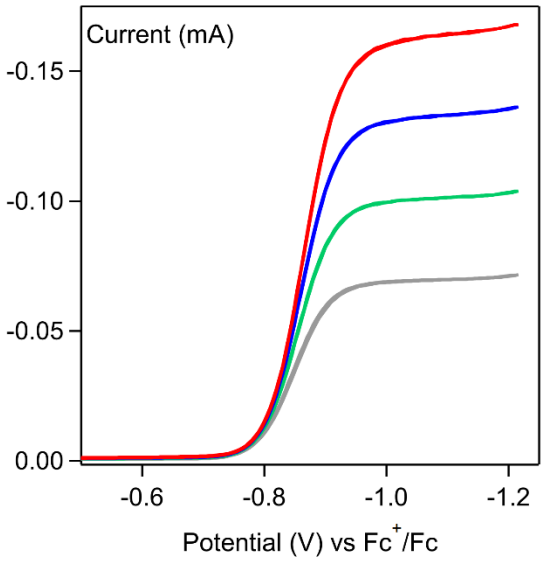

Figure S9 RDE voltammograms of 0.5 mM $Co(dmgBF_2)_2(CH_3CN)_2$ in the presence of 0.5 mM anilinium at rotation rates of 42 (grey), 94 (green), 168 (blue), and 262 (red) rad sec^{-1}. Voltammograms recorded at 0.01 V sec^{-1} in 0.25 M $[NBu_4][PF_6]$ acetonitrile using a ferrocene (0.5 mM) internal standard.

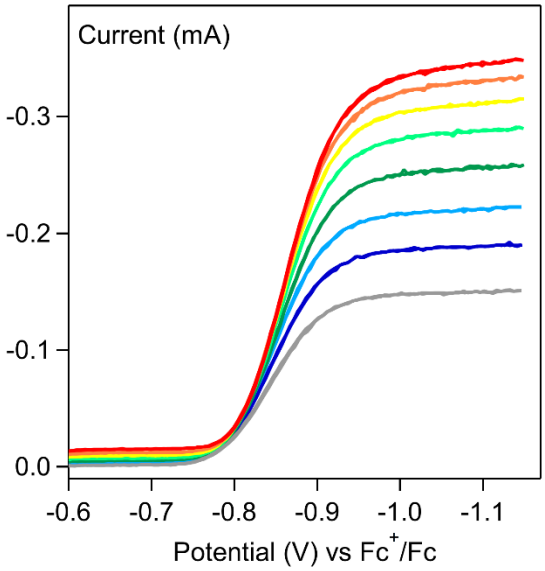

Figure S10 RDE voltammograms of 0.5 mM $Co(dmgBF_2)_2(CH_3CN)_2$ in the presence of 5 mM anilinium at rotation rates ranging of 42 (grey), 68 (dark blue), 94 (light blue), 131 (green), 168 (light green),199 (yellow), 230 (orange), and 262 rad sec^{-1} (red). Voltammograms recorded at 0.01 V sec^{-1} in 0.25 M $[NBu_4][PF_6]$ acetonitrile using a decamethylferrocene (0.25 mM) internal standard.

4-trifluoromethoxyanilinium (pK_a = 9.28)

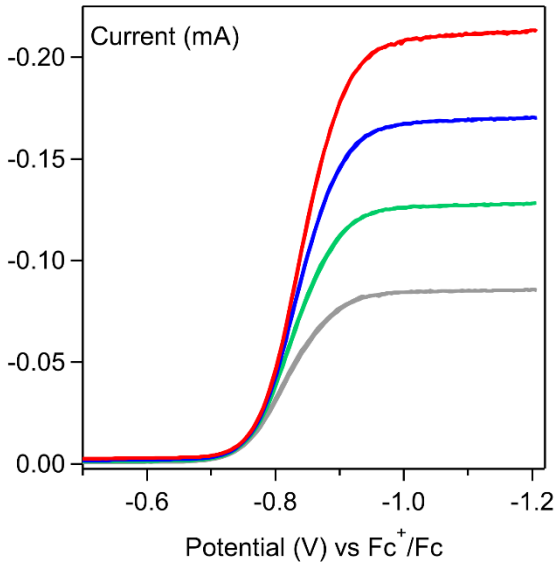

Figure S11 RDE voltammograms of 0.5 mM $Co(dmgBF_2)_2(CH_3CN)_2$ in the presence of 0.5 mM 4-trifluoromethoxyanilinium at rotation rates of 42 (grey), 94 (green), 168 (blue), and 262 (red) rad sec^{-1} (red). Voltammograms recorded at 0.01 V sec^{-1} in 0.25 M $[NBu_4][PF_6]$ acetonitrile using a ferrocene (0.5 mM) internal standard.

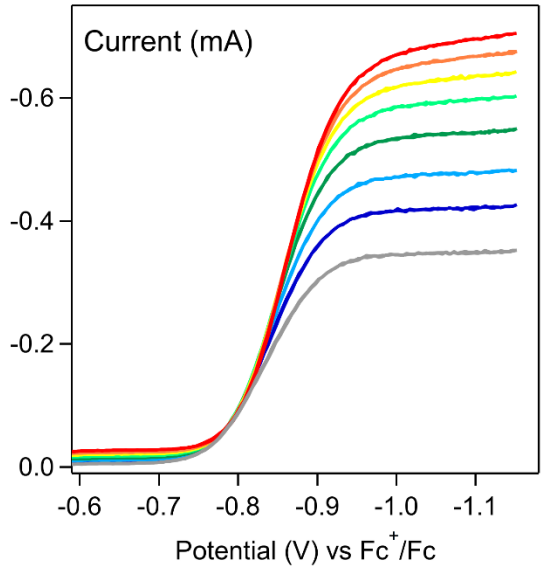

Figure S12 RDE voltammograms of 0.5 mM $Co(dmgBF_2)_2(CH_3CN)_2$ in the presence of 5 mM 4-trifluoromethoxyanilinium at rotation rates of 42 (grey), 68 (dark blue), 94 (light blue), 131 (green), 168 (light green),199 (yellow), 230 (orange), and 262 rad sec^{-1} (red). Voltammograms recorded at 0.01 V sec^{-1} in 0.25 M $[NBu_4][PF_6]$ acetonitrile using a decamethylferrocene (0.25 mM) internal standard.

SI-3 Extracting kinetic information using foot-of-the-wave analysis

To ensure that foot-of-the-wave analysis (FOWA) is applicable in RDEV, a series of digital simulations were performed and the simulated voltammograms were evaluated via the modified FOWA protocol discussed below. Rate constants used in the simulations were based on reported rates for HER by $Co(dmgBF_2)_2(CH_3CN)_2$ in the presence of 4-trifluoromethoxyanilinium (k_1 = 9.91e06 M^{-1} s^{-1}, k_2 = 3340 M^{-1} s^{-1}, k_Ω = 125 s^{-1}).[2] As HER by $Co(dmgBF_2)_2(CH_3CN)_2$ proceeds via an ECEC′ pathway where the second electron transfer is more thermodynamically favorable than the first ($E_1 < E_2$) and the first chemical step is not rate-limiting ($k_1 > k_2$), FOWA can be used to evaluate k_1.[5] As has been previously reported for FOWA for stationary cyclic voltammetry, the accuracy of the determined rate constant decreases as ΔE or k_1/k_2 becomes smaller due to the increased contribution of the second electrochemical process; in some cases, k_1 can be underestimated by order-of-magnitudes.[6] All simulations were generated in DigiElch 8.FD.

Evaluation of simulated voltammograms using FOWA

As HER by $Co(dmgBF_2)_2(CH_3CN)_2$ proceeds with a $\log(k_1/k_2)$ ratio of approximately 3.5 when using 4-trifluoromethoxyanilinium, a ΔE greater than approximately -0.25 V is necessary to ensure that rate information extracted through FOWA is within an order of magnitude of true rate constant of the first chemical step.[2,6] However, the reduction potential of Co(III)-H is estimated to be only 20-100 mV more positive than the $Co^{II/I}$ couple and thus any k_1 value determined by FOWA is expected to underestimate the true value.[7,8] As such, three series of simulations were performed which set the ΔE values as either 20 mV, 100 mV, or 400 mV. Rate constants derived for all simulations are within an order of magnitude of the input k_1 value and, as expected, the determined k_1 value for simulations using ΔE values of 20 and 100 mV underestimate the input k_1 value.

Parameters for digital simulations

Scan Rate	Geometry	Radius	Potential Steps	R_u	Temp	Cdl
0.001 V/s	Planar	0.25 cm	0.001 V	0 ohm	298.2 K	0

Diffusion	Rotation Rate	v
Hydrodynamic	100 rad s^{-1}	0.00455 cm^2/s

Charge Transfer Reactions:

Reaction	$E^{o\prime}$	α	k_s
Co(II) + e^- ⇌ Co(I)	0 V	0.5	10000 cm/s
CoH + e^- ⇌ CoH-	varied	0.5	10000 cm/s

***E*°′** for CoH/CoH^- redox couple varied between 0.02, 0.1, and 0.4 V

Chemical Reactions:

Reaction	*k*
Co(I) + H ⟶ CoH	9.91e06 M s^{-1}
CoH- + H ⟶ CoH2	3340 M s^{-1}
CoH2 ⟶ Co(II) + H2	125 s^{-1}

Species Parameters:

	D	Initial Concentration
Co(II)	1e-05 cm^2/s	0.0005 M
Co(I)	1e-05 cm^2/s	0 M
acid	1e-05 cm^2/s	Varied
CoH	1e-05 cm^2/s	0 M
CoH-	1e-05 cm^2/s	0 M
CoH2	1e-05 cm^2/s	0 M
H2	1e-05 cm^2/s	0 M

Initial concentration of acid varied between 0, 0.005, 0.025, and 0.05 M

To perform FOWA, the potential axis of the catalytic voltammogram was converted to $1/(1+\exp[\theta])$ and the current (i_c) was divided by the plateau current of the $Co^{II/I}$ wave in the absence of acid (i_p). The resulting plots of i_c/i_p vs $1/(1+\exp[\theta])$ are linear near the foot of the catalytic wave. To extract an observed rate constant (k_{FOWA}) from the slope of the linear region, the equation derived for FOWA of an ECEC′ mechanism (equation S2 and SI-4, Supporting Information I) is divided by the Levich equation (equation S1) to yield an i_c/i_p relationship (equation S3) that can be used to obtain k_{FOWA}.

$$i_c = \frac{2FAC_P^0\sqrt{k_{FOWA}D_{cat}}}{1+exp[\theta]} \qquad \text{(S2)}$$

$$\frac{i_c}{i_p} = \frac{3.22}{n}\left(\frac{\nu}{D}\right)^{1/6}\sqrt{\frac{k_{FOWA}}{\omega}}\left[\frac{1}{1+\exp[\theta]}\right] \qquad \text{(S3)}$$

Case 1: $E^{o\prime}$ of CoH/CoH$^-$ redox couple = 0.02 V

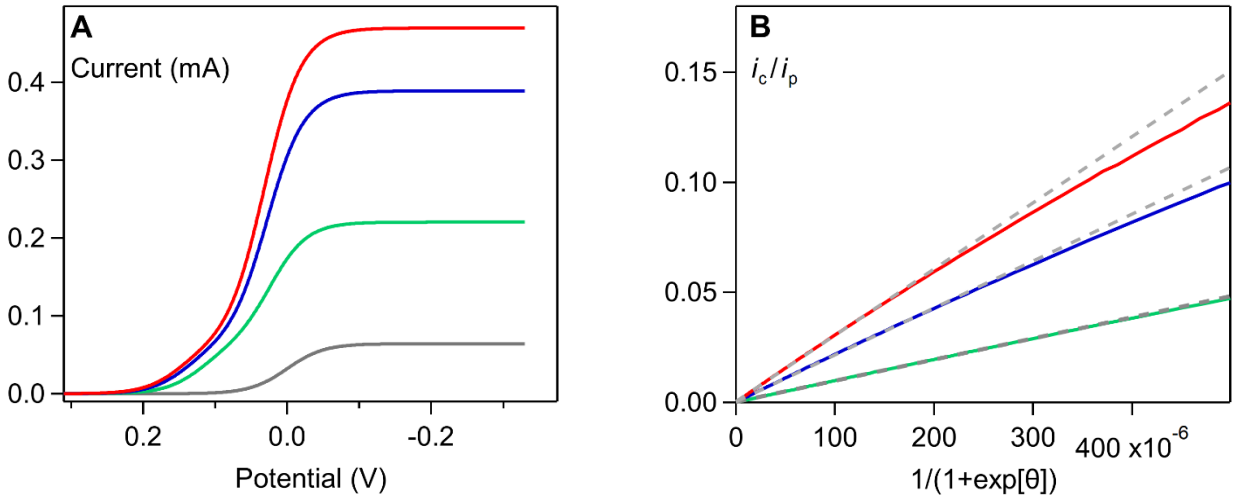

Figure S13 (A) Simulation of ECEC′ mechanism for Δ*E* = 0.02 V when C_A^0 is 0 M (grey), 0.005 M (green), 0.025 M (blue), or 0.05 M (red). **(B)** FOW plot obtained by converting the current to the i_c/i_p ratio and converting potential to the FOW axis 1/(1+exp[θ]). Solid lines represent converted trace and are color-coded to correspond with their simulated voltammogram. Grey dashed are the linear fit of the foot of the wave.

[acid]	Slope	k_{FOWA}
0.005 M	96.2	1.16e04 s^{-1}
0.025 M	213.27	5.68e04 s^{-1}
0.05 M	301.4	1.14e05 s^{-1}

Case 2: $E^{o\prime}$ of CoH/CoH$^-$ redox couple = 0.1 V

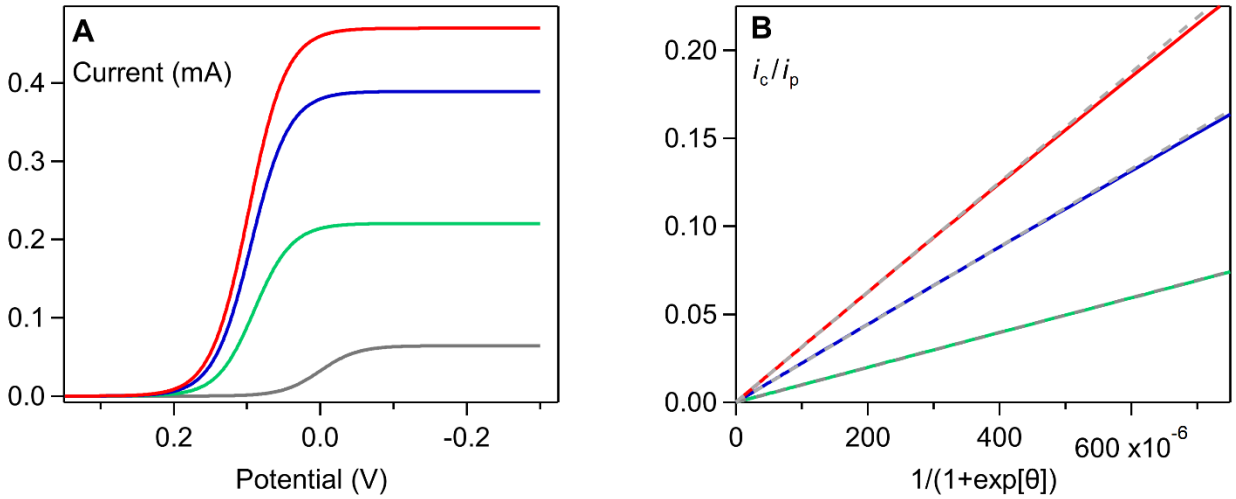

Figure S14 (A) Simulation of ECEC′ mechanism for Δ*E* = 0.1 V when C_A^0 is 0 M (grey), 0.005 M (green), 0.025 M (blue), or 0.05 M (red). **(B)** FOW plot obtained by converting the current to the i_c/i_p ratio and converting potential to the FOW axis 1/(1+exp[θ]). Solid lines represent converted trace and are color-coded to correspond with their simulated voltammogram. Grey dashed lines are the linear fit of the foot of the wave.

[acid]	Slope	k_{FOWA}
0.005 M	98.9	1.22e04 s^{-1}
0.025 M	220.9	6.10e04 s^{-1}
0.05 M	312.0	1.22e05 s^{-1}

Case 3: $E^{o\prime}$ of CoH/CoH$^-$ redox couple = 0.4 V

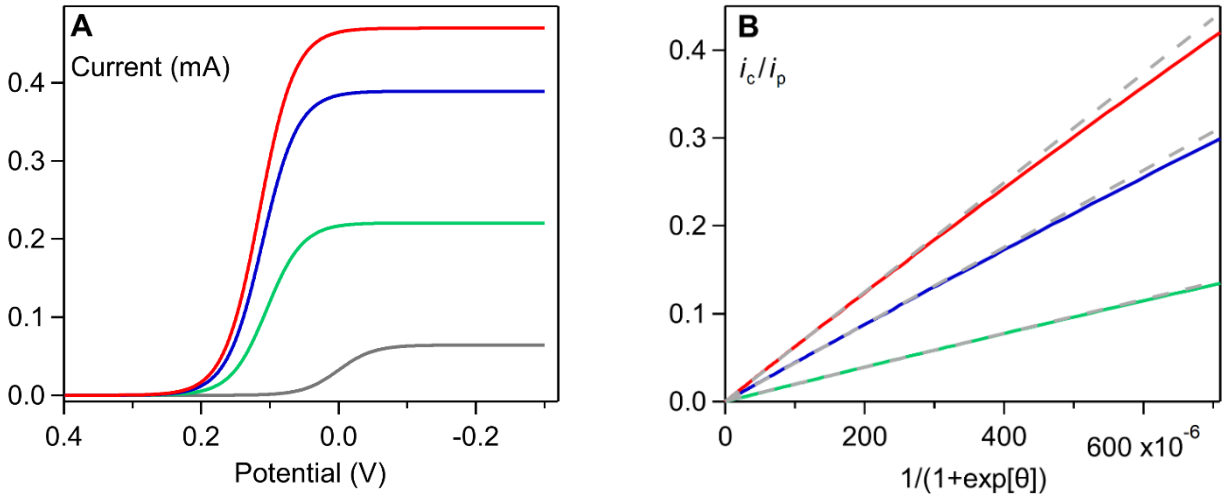

Figure S15 (A) Simulation of ECEC′ mechanism for Δ*E* = 0.4 V when C_A^0 is 0 (grey), 0.005 (green), 0.025 (blue), or 0.05 M (red). **(B)** FOW plot obtained by converting the current to the i_c/i_p ratio and converting potential to the FOW axis. Solid lines represent converted trace and are color-coded to correspond with their simulated voltammogram. Grey dashed lines are the linear fit of the FOW.

[acid]	Slope	k_{FOWA}
0.005 M	193.0	4.66e04 s^{-1}
0.025 M	438.16	2.40e05 s^{-1}
0.05 M	622.37	4.84e05 s^{-1}

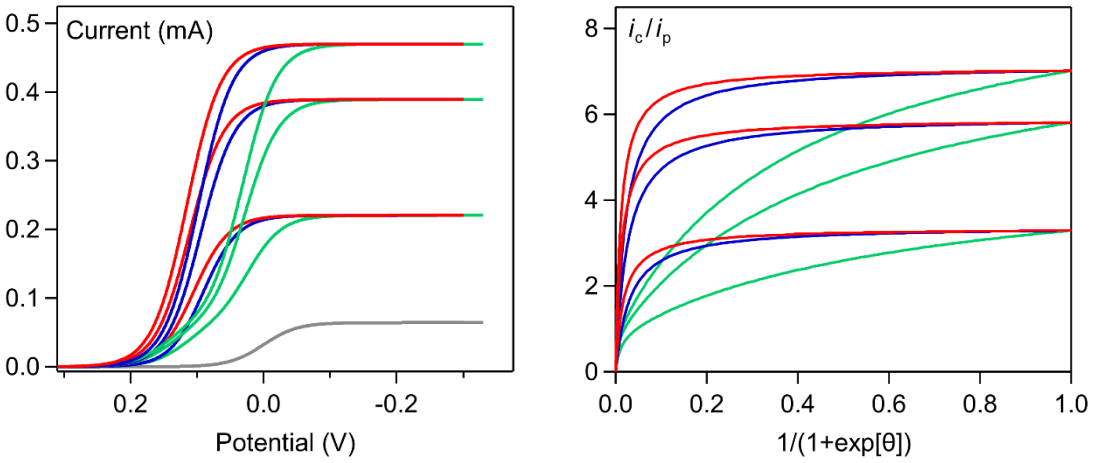

Figure S16 (Left) Comparison of simulated voltammograms with Δ*E* = 0.02 (green), 0.1 (blue), and 0.4 (red) V and [substrate] of 0 (grey), 0.005, 0.025, and 0.05 M. **(Right)** Comparison of corresponding FOW plots. Traces are color coded to correspond with their simulated voltammogram.

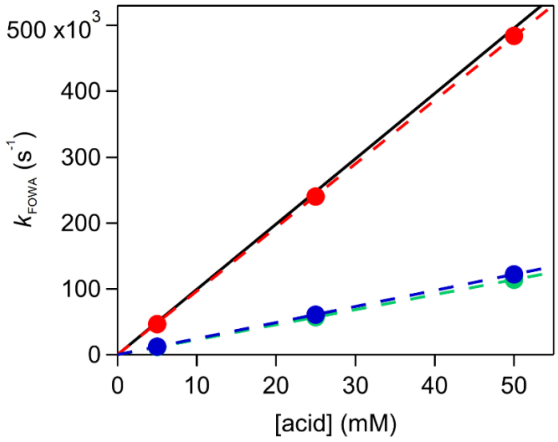

Figure S17 k_1 was extracted from the slope of k_{FOWA} versus [acid] ($k_{FOWA} = k_1$[acid]). Dots represent k_{FOWA} for simulated data with Δ*E* values of 0.02 (green), 0.1 (blue), and 0.4 (red) V. Dashed lines are linear fits of k_{FOWA} data and are color-coded to correspond with their data points. Solid black line represents the ideal linear fit for k_1 = 9.91e06 M^{-1} s^{-1}.

Rate constants calculated using FOWA

Δ*E* (mV)	**k_1 (M^{-1} s^{-1})**
20	2.28e06
100	2.44e06
400	9.66e06

Impact of relative rate constants on FOWA for simulated voltammograms

A second parameter that has been shown to impact the accuracy of k_1 values extracted from FOWA for an ECEC′ in the context of stationary CV is the ratio of the rate constants for the two chemical steps (k_1/k_2), with smaller k_1/k_2 values resulting in greater underestimations of k_1 due to increased contribution of the second electrochemical process.[6] To explore the impact of this ratio on FOWA for RDEV, two sets of simulations were conducted. First, a generic ECEC′ mechanism with log(k_1/k_2) values spanning a range from 1 to 3 was analyzed. These simulations show that a comparable dependence of the accuracy of k_1 on the ratio of k_1/k_2 will be operative in FOWA for RDEV. To determine the extent that this ratio will impact analysis of experimental data, FOWA was applied to simulations using kinetic parameters specific to HER by $Co(dmgBF_2)_2(CH_3CN)_2$ with *para*-substituted anilinium. In all simulations, the Δ*E* value was set to 0.4 V in order to minimize any convoluting influence from this parameter.

Simulation Set 1: Generic simulations of an ECEC′ mechanism

Parameters for digital simulations

Scan Rate	Geometry	Radius	Potential Steps	R_u	Temp	Cdl
0.001 V/s	Planar	0.25 cm	0.001 V	0 ohm	298.2 K	0

Diffusion	Rotation Rate	v
Hydrodynamic	100 rad s^{-1}	0.00455 cm^2/s

Charge Transfer Reactions:

Reaction	$E^{o\prime}$	α	k_s
$P + e^- \rightleftharpoons Q$	0 V	0.5	10000 cm/s
$QA + e^- \rightleftharpoons QA^-$	0.4 V	0.5	10000 cm/s

Chemical Reactions:

Reaction	*k*
Q + acid ⟶ QA	varied
QA- + acid ⟶ P + B	10 M s^{-1}

k_1 varied between 100, 1000, and 10000 M^{-1} sec^{-1}

Species Parameters:

	D	Initial Concentration
P	1e-05 cm^2/s	0.0005 M
Q	1e-05 cm^2/s	0 M
acid	1e-05 cm^2/s	Varied
QA	1e-05 cm^2/s	0 M
QA-	1e-05 cm^2/s	0 M
B	1e-05 cm^2/s	0 M

Initial concentration of acid varied between 0, 0.025, 0.05, and 0.5 M

Case 1: $\log(k_1/k_2) = 1$

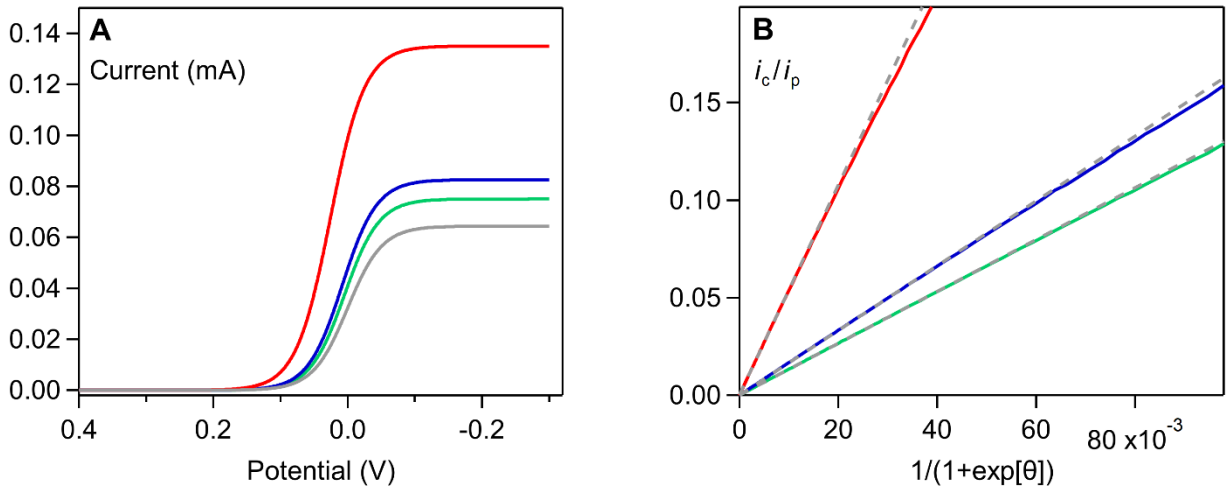

Figure S18 (A) Simulation of ECEC′ mechanism for $\log(k_1/k_2) = 1$ when C_A^0 is 0 (grey), 0.025 (green), 0.05 (blue), or 0.5 M (red). **(B)** FOW plot obtained by converting the current to the i_c/i_p ratio and converting potential to the FOW axis 1/(1+exp[θ]). Solid lines represent converted trace and are color-coded to correspond with their simulated voltammogram. Grey dashed lines are the linear fit of the foot of the wave.

[acid]	Slope	k_{FOWA}
0.025 M	1.33	2.21 s^{-1}
0.05 M	1.66	3.45 s^{-1}
0.5 M	5.38	3.63 s^{-1}

Case 2: log(k_1/k_2) = 2

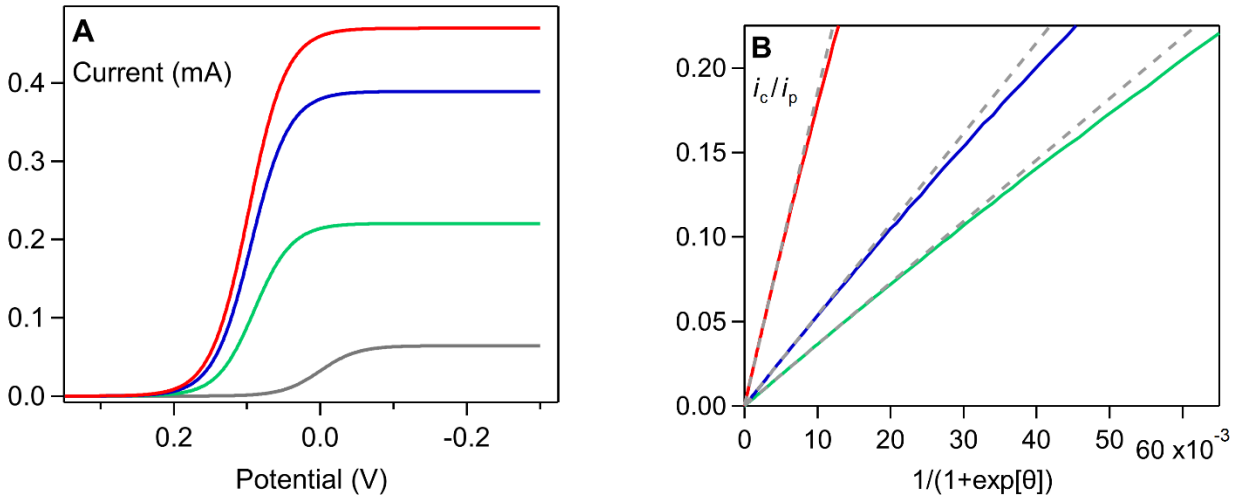

Figure S19 (A) Simulation of ECEC′ mechanism for log(k_1/k_2) = 2 when C_A^0 is 0 (grey), 0.025 (green), 0.05 (blue), or 0.5 M (red). **(B)** FOW plot obtained by converting the current to the i_c/i_p ratio and converting potential to the FOW axis 1/(1+exp[θ]). Solid lines represent converted trace and are color-coded to correspond with their simulated voltammogram. Grey dashed lines are the linear fit of the foot of the wave.

[acid]	Slope	k_{FOWA}
0.025 M	3.64	1.66e01 s^{-1}
0.05 M	5.37	3.61e01 s^{-1}
0.5 M	18.5	4.31e02 s^{-1}

Case 3: log(k_1/k_2) = 3

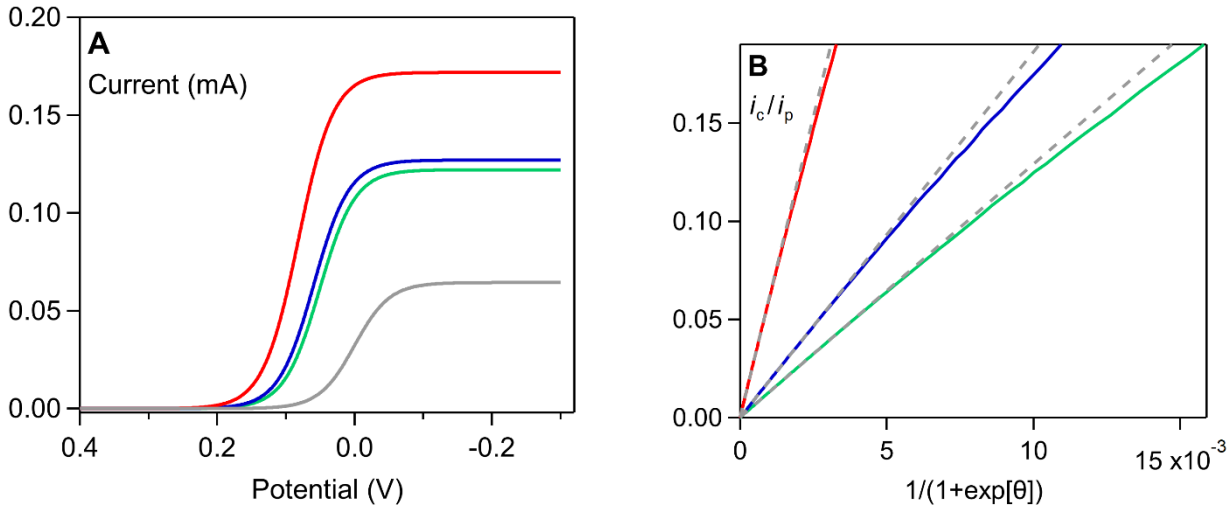

Figure S20 (A) Simulation of ECEC′ mechanism for log(k_1/k_2) = 3 when C_A^0 is 0 (grey), 0.025 (green), 0.05 (blue), or 0.5 M (red). **(B)** FOW plot obtained by converting the current to the i_c/i_p ratio and converting potential to the FOW axis 1/(1+exp[θ]). Solid lines represent converted trace and are color-coded to correspond with their simulated voltammogram. Grey dashed lines are the linear fit of the foot of the wave.

[acid]	Slope	k_{FOWA}
0.025 M	12.9	2.08e02 s^{-1}
0.05 M	18.6	4.34e02 s^{-1}
0.5 M	61.2	4.69e03 s^{-1}

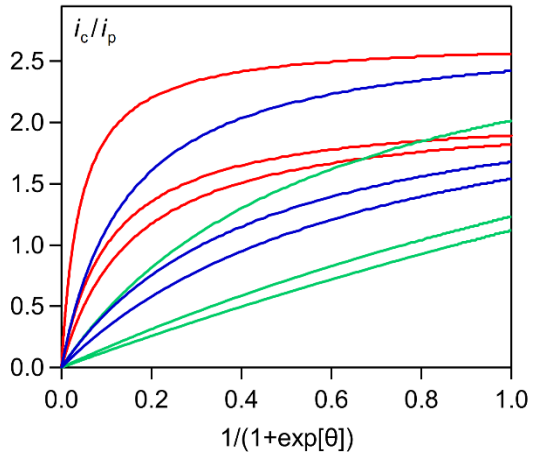

Figure S21 Comparison of FOW plots derived from simulated voltammograms with log(k_1/k_2) = 1 (green), 2 (blue), and 3 (red) and [substrate] of 0.025, 0.05, and 0.5 M.

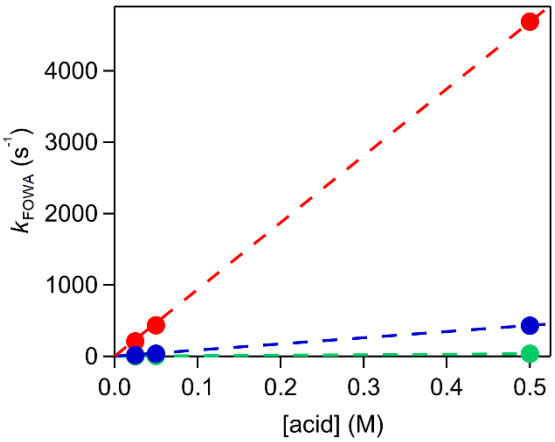

Figure S22 k_1 was extracted from the slope of k_{FOWA} versus [acid] ($k_{FOWA} = k_1$[acid]). Dots represent k_{FOWA} for simulated data with log(k_1/k_2) = 1 (green), 2 (blue), and 3 (red). Dashed lines are linear fits of k_{FOWA} data and are color-coded to correspond with their data points.

Rate constants calculated using FOWA

log(k_1/k_2)	**k_1 (M^{-1} s^{-1})**	**k_{1_FOWA} (M^{-1} s^{-1})**	**log(k_{1_FOWA}/k_1)**
1	100	72.6	-0.14
2	1000	861	-0.065
3	10000	9374	-0.028

Simulation Set 2: Simulations of HER by $Co(dmgBF_2)_2(CH_3CN)_2$ with *para*-substituted aniliniums

For HER by $Co(dmgBF_2)_2(CH_3CN)_2$, the k_1/k_2 ratio will depend on the identity of the acid with $\log(k_1/k_2)$ values ranging from 2.95 (4-methoxyanilinium) to 3.52 (4-methylbenzoateanilinium) if the second protonation step is rate-limiting. For acids where the acid independent step (k_Ω) becomes rate-limiting at high acid concentrations, this ratio will range from 4.90 (4-trifluoromethoxyanilinium) to 6.34 (4-cyanoanilinium). To explore the extent that these ratios will impact FOWA for $Co(dmgBF_2)_2(CH_3CN)_2$ with *para*-substituted aniliniums, simulations were performed using the previously reported rate constants for 4-methoxyanilinium and the accuracy of these results were compared to the analogous simulations performed using the reported rate constants for 4-trifluoromethoxyanilinium (see **Figure S*15***, **Figure S*17***).[2]

Parameters for digital simulations

Scan Rate	Geometry	Radius	Potential Steps	R_u	Temp	Cdl
0.001 V/s	Planar	0.25 cm	0.001 V	0 ohm	298.2 K	0

Diffusion	Rotation Rate	v
Hydrodynamic	100 rad s^{-1}	0.00455 cm^2/s

Charge Transfer Reactions:

Reaction	$E^{o\prime}$	α	k_s
Co(II) + e^- ⇌ Co(I)	0 V	0.5	10000 cm/s
CoH + e^- ⇌ CoH-	0.4 V	0.5	10000 cm/s

Chemical Reactions:

Reaction	*k*
Co(I) + H ⟶ CoH	3.06e04 M s^{-1}
CoH- + H ⟶ CoH2	33.9 M s^{-1}
CoH2 ⟶ Co(II) + H2	125 s^{-1}

Species Parameters:

	D	Initial Concentration
Co(II)	1e-05 cm^2/s	0.0005 M
Co(I)	1e-05 cm^2/s	0 M
acid	1e-05 cm^2/s	Varied
CoH	1e-05 cm^2/s	0 M
CoH-	1e-05 cm^2/s	0 M
CoH2	1e-05 cm^2/s	0 M
H2	1e-05 cm^2/s	0 M

Initial concentration of acid varied between 0, 0.005, 0.025, and 0.05 M

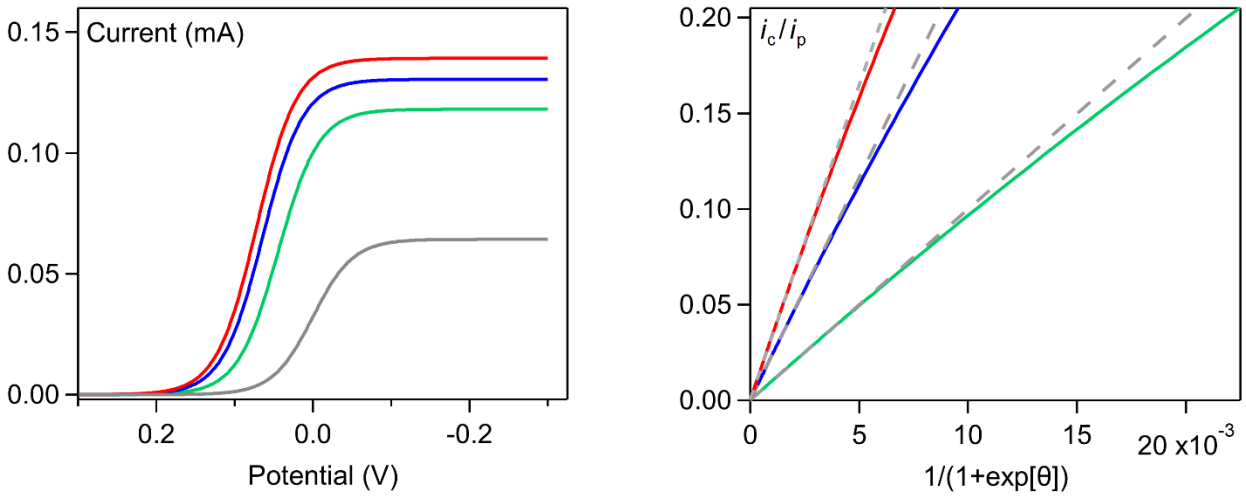

Figure S23 (left) Simulation of ECEC′ mechanism using the kinetic parameters for 4-methoxyanilinium when C_A^0 is 0 M (grey), 0.005 M (green), 0.025 M (blue), or 0.05 M (red). **(right)** FOW plot obtained by converting the current to the i_c/i_p ratio and converting potential to the FOW axis 1/(1+exp[θ]). Solid lines represent converted trace and are color-coded to correspond with their simulated voltammogram. Grey dashed lines are the linear fit of the foot of the wave.

[acid]	Slope	k_{FOWA}
0.005 M	9.98	1.24e02 s^{-1}
0.025 M	23.21	6.73e02 s^{-1}
0.05 M	32.84	1.34e03 s^{-1}

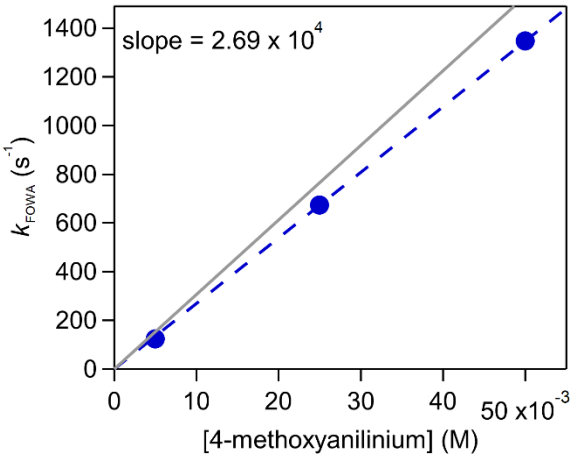

Figure S24 k_1 was extracted from the slope of k_{FOWA} versus [acid] ($k_{FOWA} = k_1$[acid]). Dots represent k_{FOWA} for simulated data and dashed lines are linear fits of k_{FOWA} data. Solid grey line represents the ideal linear fit for k_1 = 3.06e04 M^{-1} s^{-1}.

Comparison of rate constants for 4-methoxyanilinium and 4-trifluoromethoxyanilinium (ΔE = 0.4 V)

	k_{1_FOWA} (M^{-1} s^{-1})	reported k_1 (M^{-1} s^{-1})	log(k_{1_FOWA}/k_1)
4-methoxyanilinium	2.67e04	3.06e04	-0.06
4-trifluoromethoxyanilinium	9.66e06	9.91e06	-0.01

Rate constants for the first chemical step derived from FOWA (k_{1_FOWA}) are within an order of magnitude of the k_1 values used in the simulations. Comparing the log(k_{1_FOWA}/k_1) for the two acids shows that a slightly more accurate rate constant is extracted from simulations using the reported rate constants for HER with 4-trifluoromethoxyanilinium, behavior consistent with the larger k_1/k_2 ratio under these conditions, however the relative impact is negligible.

Application of FOWA to experimental data

FOWA was applied to RDE voltammograms recorded with 0.5 mM $Co(dmgBF_2)_2(CH_3CN)_2$ in the presence of 4-trifluoromethoxyanilinium (RDE voltammograms and FOW traces available in the main text). Data sets used for FOWA were obtained with a freshly polished electrode using a fresh solution of catalyst and acid in order to minimize interference from side phenomena. To perform FOWA, the potential axis of the voltammogram was converted to $1/(1+\exp[\theta])$ and the current (i_c) was divided by the plateau current of the $Co^{II/I}$ wave in the absence of acid (i_p).

An observed rate constant (k_{FOWA}) was extracted from the slope of the linear region at the FOW using equation S3. In this work, the number of electrons passed in the Levich equation is n = 1. All data sets collected at ω = 42 rad sec^{-1}. The values of k_{FOWA} were found to linearly depend on acid concentration, allowing a k_1 of 8.42e06 M^{-1} s^{-1} to be calculated.

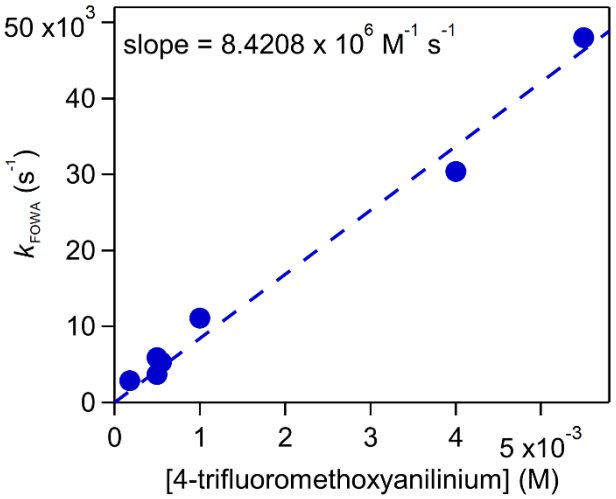

Figure S25 Observed rate constants derived via FOWA as a function of acid concentration. The linear dependence of this plot allowed the rate constant for the first chemical step to be estimated.

SI-4 Evolution of Solution Composition

RDE voltammograms (3 voltammograms per rotation rate) were collected in a Fc-only solution at five rotation rates (42, 94, 168, 262, 316 rad sec^{-1}) and OCP measurements were obtained between each voltammogram (see section 3.3.1). During these voltammograms, the potential was first scanned positively until a limiting cathodic current (corresponding to the oxidation of ferrocene) was reached (ca. 0.4 V) at which point the scan direction was switched and the potential was scanned negatively until a baseline current was reached (ca. -0.45 V). Voltammograms recorded at 0.005 V s^{-1} in 0.25 M $[NBu_4][PF_6]$ acetonitrile and are available in the main text.

Figure S26 Picture of electrochemical cell containing 2 mM ferrocene in 0.25 M $[NBu_4][PF_6]$ acetonitrile following final RDEV-OCP measurement. Solution color changed from orange – as expected for ferrocene – to green over the course of the scans.

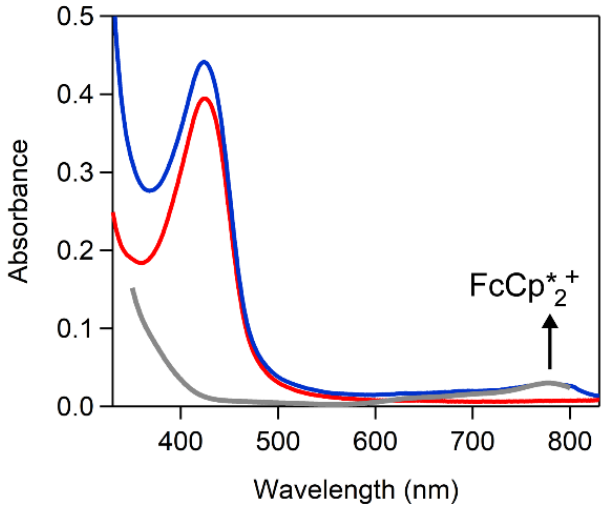

Figure S27 UV-vis absorbance spectra tracking the composition of the solution during variable rotation rate trials using 0.5 mM $Co(dmgBF_2)_2(CH_3CN)_2$ with 5 mM anilinium and 0.5 mM decamethylferrocene in 0.25 M $[NBu_4][PF_6]$ acetonitrile (see **Figure S10**). Two spectra were collected at the end of the RDE experiments: (red) an aliquot of the solution that had not undergone any electrochemical trials and (blue) the reaction solution after variable rotation rate experiments. Growth of a feature at 775 nm consistent with features observed for decamethylferrocenium (grey trace) can be observed in the spectrum of the reaction solution after variable rotation rate experiments.

SI-5 Electrochemical Monitoring of Electrode Properties

Intermediate stationary voltammograms recorded during variable rotation rate trials

For variable rotation rate studies in solutions of 0.5 mM $Co(dmgBF_2)_2(CH_3CN)_2$ with 5 mM acid, the rotator was turned off between each RDE trial and stationary voltammograms were recorded in the same solution using the same working electrode without polishing between scans. For all stationary catalytic voltammograms recorded, the catalytic wave is peak-shaped and the current does not reach a plateau. For these stationary catalytic voltammograms, Ψ^{∞} is defined as (catalytic peak current)/i_{peak}. Plots tracking the peak-to-peak separation for the $Co^{III/II}$ couple and the Ψ^{∞} values for the stationary voltammograms are plotted as a function of the rotation rate for the RDE trial collected prior to the stationary voltammogram. Rotation rates were traversed in ascending order, such that moving from left to right across the x-axis represents both an increase in ω and trial number.

4-trifluoromethoxyanilinium

Pertinent RDE voltammograms and stationary voltammograms of 0.5 mM $Co(dmgBF_2)_2(CH_3CN)_2$ with 5 mM 4-trifluoromethoxyanilinium can be found in the main text in Figure 16 and 18, respectively.

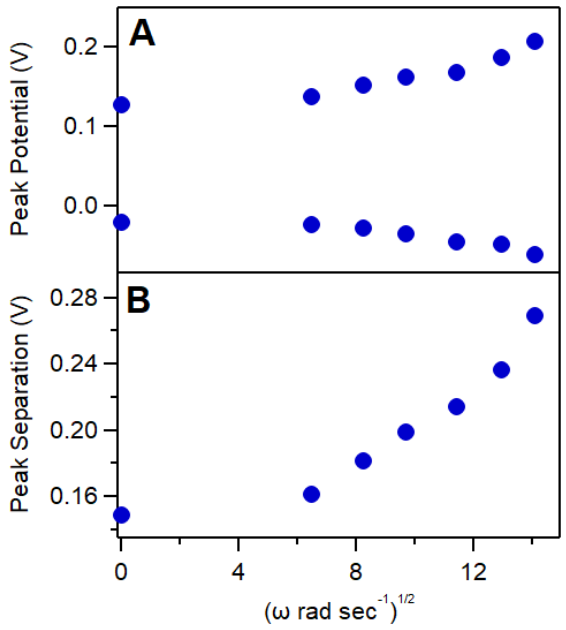

Figure S28 (A) Potentials (vs. $Fc^{+/0}$) for the anodic and cathodic peaks of the $Co^{III/II}$ couple across variable rotation rate trials in a solution of 0.5 mM $Co(dmgBF_2)_2(CH_3CN)_2$ with 5 mM 4-trifluoromethoxyanilinium and 0.25 mM decamethylferrocene along with **(B)** their respective peak-to-peak separation.

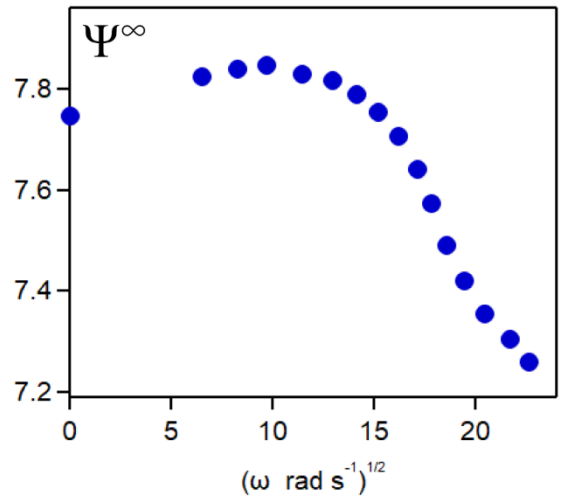

Figure S29 Variation of Ψ^{∞} for stationary voltammograms over the course of rotation rate studies in a solution of 0.5 mM $Co(dmgBF_2)_2(CH_3CN)_2$ with 5 mM 4-trifluoromethoxyanilinium and 0.25 mM decamethylferrocene.

Anilinium

Pertinent stationary voltammograms of 0.5 mM $Co(dmgBF_2)_2(CH_3CN)_2$ with 5 mM anilinium along with plots tracking changes in Ψ^{∞} and $\Delta E_p[Co^{III/II}]$ can be found in the main text in Figure 19. For RDE voltammograms, a two-segment potential range that included the $[Fc^*]^{+/0}$ couple was used: the potential

was swept from -0.25 V to -1.15 V and then from -1.15 V back to -0.25 V. Because this range includes the $[Fc^*]^{+/0}$ couple, the increase in baseline current observed during RDE measurements is attributed to the accumulation of the oxidized internal standard decamethylferrocenium in solution.

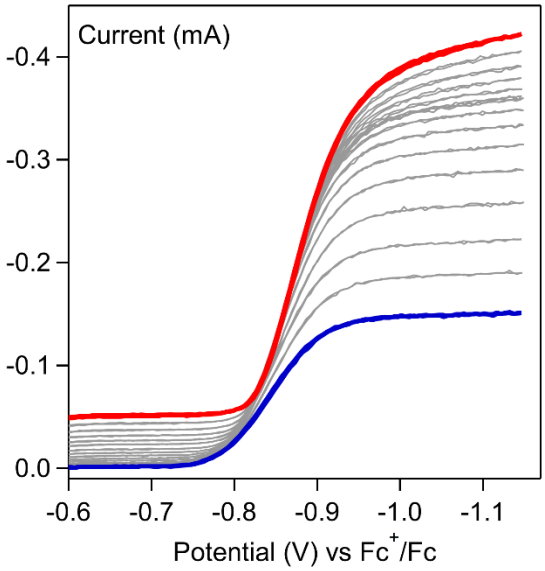

Figure S30 RDE voltammograms of 0.5 mM $Co(dmgBF_2)_2(CH_3CN)_2$ in the presence of 5 mM anilinium at rotation rates ranging from 42 rad sec^{-1} (blue) to 513 rad sec^{-1} (red). Voltammograms recorded at 0.01 V sec^{-1} in 0.25 M $[NBu_4][PF_6]$ acetonitrile using a decamethylferrocene (0.25 mM) internal standard.

4-methoxyanilinium

Voltammograms were recorded using a ferrocene internal standard which partially overlapped with the $Co^{III/II}$ redox couple, precluding analysis of the change in peak-to-peak separation for this wave. For RDE voltammograms, a three-segment potential range that included the $Fc^{+/0}$ couple was used: the potential was swept from -0.25 V to -1.15 V, then from -1.15 V to 0.2 V, and finally from 0.2 V back to -0.25 V. Because this range includes the $Fc^{+/0}$ couple, the increase in baseline current observed during RDE measurements is attributed to the accumulation of the oxidized internal standard ferrocenium in solution.

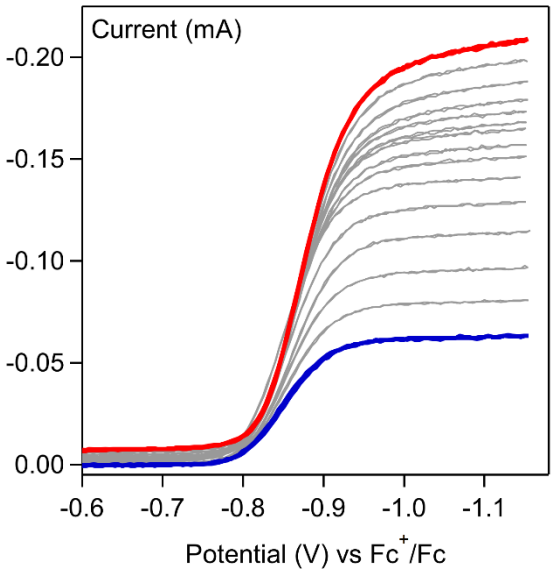

Figure S31 RDE voltammograms of 0.5 mM $Co(dmgBF_2)_2(CH_3CN)_2$ in the presence of 5 mM 4-methoxyanilinium at rotation rates ranging from 42 rad sec^{-1} (blue) to 513 rad sec^{-1} (red). Voltammograms recorded at 0.01 V sec^{-1} in 0.25 M $[NBu_4][PF_6]$ acetonitrile using a ferrocene (0.5 mM) internal standard.

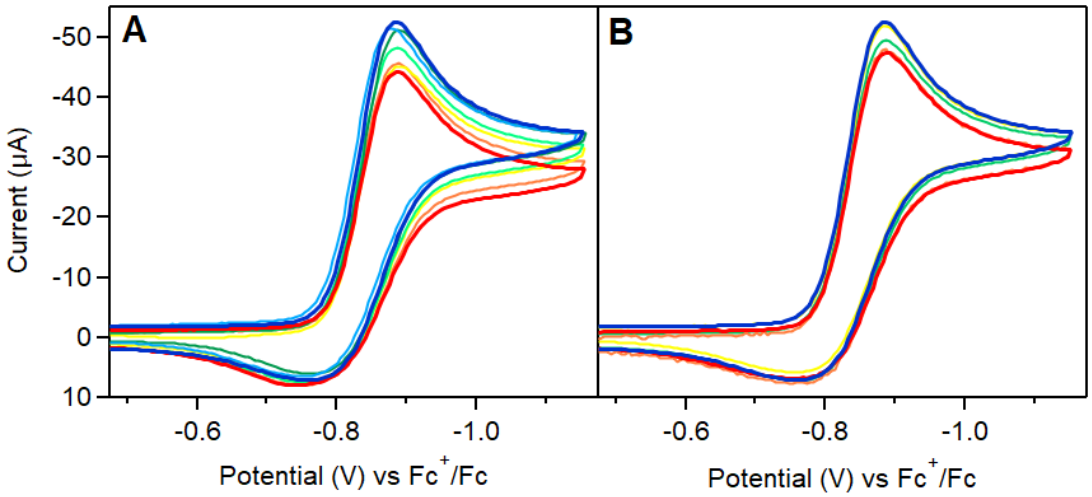

Figure S32 Stationary voltammograms of 0.5 mM $Co(dmgBF_2)_2(CH_3CN)_2$ in the presence of 5 mM 4-methoxyanilinium with a ferrocene (0.5 mM) internal standard. Voltammograms recorded at 0.1 V s^{-1} in 0.25 M $[NBu_4][PF_6]$ acetonitrile. **(A)** Voltammogram collected prior to RDE trials in red. Peak current increases in stationary voltammogram collected after RDE trials recorded at 42 (orange), 68 (yellow), 94 (light green), 131 (dark green), 168 (light blue), and 199 (dark blue) rad sec^{-1}. **(B)** Voltammogram collected after 199 rad sec^{-1} again shown in dark blue. Lower peak currents observed for stationary scans recorded after RDE trials at 230 (green), 262 (yellow), 293 (orange), and 317 rad sec^{-1} (red).

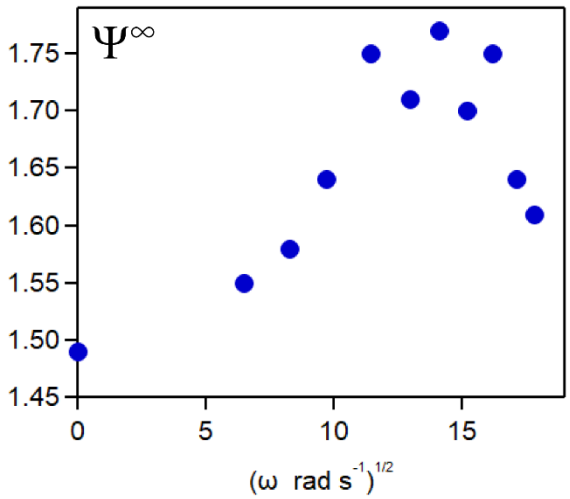

Figure S33 Variation of Ψ^{∞} for stationary voltammograms over the course of rotation rate studies in a solution of 0.5 mM $Co(dmgBF_2)_2(CH_3CN)_2$ with 5 mM 4-methoxyanilinium and 0.5 mM ferrocene.

Evaluating electrode modification in the absence of RDEV

To evaluate whether electrode modification is also observable in stationary experiments collected under conditions similar to those employed in RDE voltammetry, two control studies were conducted.

Control Study 1: Electrodeposition during catalytic trials

Multiple cycling experiments were conducted with a solution of 0.5 mM $Co(dmgBF_2)_2(CH_3CN)_2$ in the presence of 5 mM 4-trifluoromethoxyanilinium to evaluate whether the properties of the electrode interface can be observably altered over the course of stationary catalytic runs. The same working electrode was used to collect 12 stationary voltammograms in the same solution without polishing between trials. No change in the peak-to-peak separation of the $Co^{III/II}$ redox couple or consistent change in the catalytic current was observed during these trials, suggesting that observable electrode modification under catalytic conditions is unique to RDEV.

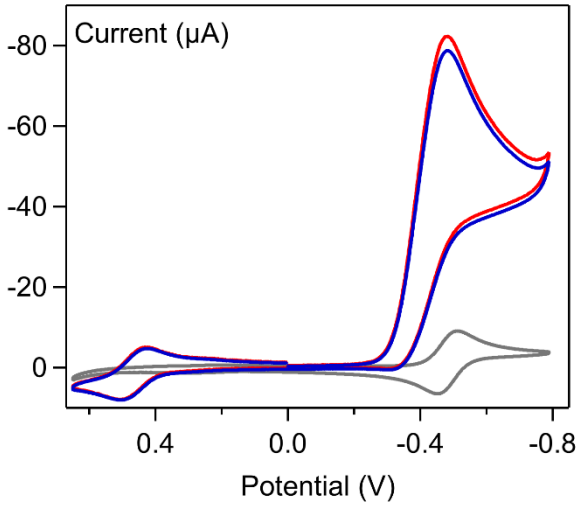

Figure S34 Stationary cyclic voltammograms of 0.5 mM $Co(dmgBF_2)_2(CH_3CN)_2$ in the absence of substrate (grey trace) and in the presence of 10 equivalents of 4-trifluoromethoxyanilinium collected with a freshly pretreated electrode (red trace) and the same electrode after multiple cycling trials (blue trace). Voltammograms recorded at 0.1 V s^{-1} in 0.25 M $[NBu_4][PF_6]$ acetonitrile using a 3 mm OD glassy carbon working electrode.

Control Study 2: Acid-induced electrodeposition

To determine whether observable electrode fouling takes place during stationary voltammograms in the presence of acid, a series of 8 stationary voltammograms were collected in a solution of 1.25 mM 4-

trifluoromethoxyanilinium with 0.25 mM decamethylferrocene internal standard (**Figure 35A**). After these multiple cycling experiments, the electrode was then rinsed with acetonitrile and used to obtain a catalytic voltammogram under stationary conditions in a solution of 0.5 mM $Co(dmgBF_2)_2(CH_3CN)_2$ with 5 mM 4-trifluoromethoxyanilinium and 0.25 mM decamethylferrocene (**Figure 35B**). In these catalytic voltammograms, an increase in $\Delta E[Co^{III/II}]$ of approximately 35 mV was observed relative to the voltammograms collected with a freshly polished electrode. However, the magnitude of the increase in $\Delta E[Co^{III/II}]$ is far smaller than that observed after analogous multiple cycling experiments collected under hydrodynamic conditions. This control studies indicates that the degree of acid-induced fouling is more pronounced during hydrodynamic experiments.

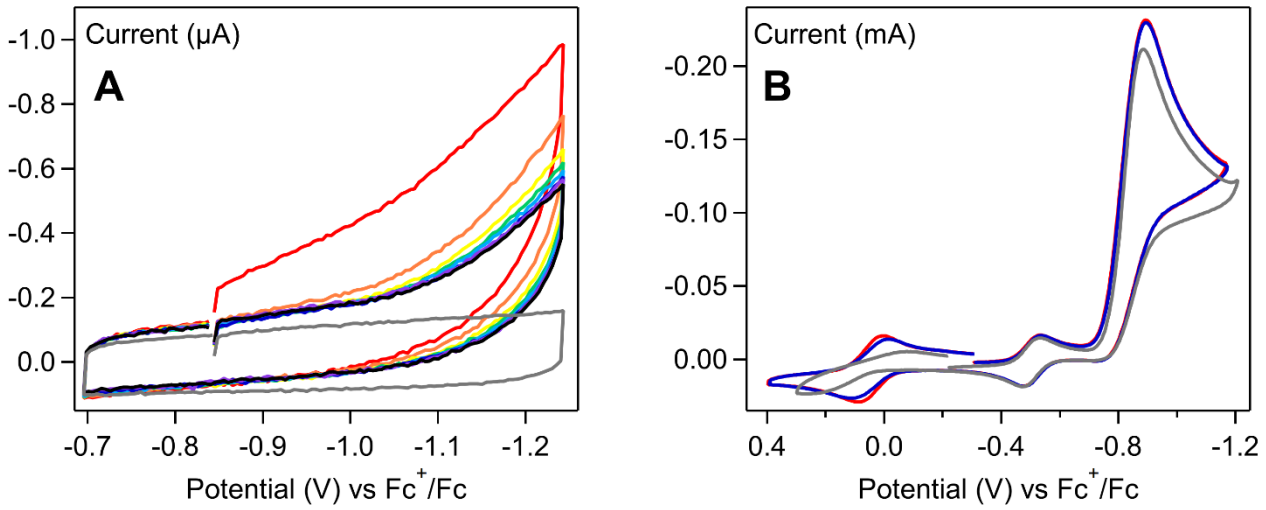

Figure S35 (A) Stationary voltammograms for multiple cycling experiments in a solution of 1.25 mM 4-trifluoromethoxyanilinium with 0.25 mM decamethylferrocene recorded in 0.25 M $[NBu_4][PF_6]$ acetonitrile at 0.01 V s^{-1}. Traces corresponding to the eight successive voltammograms that were collected in the presence of 4-trifluoromethoxyanilinium – scan 1 (red), 2 (orange), 3 (yellow), 4 (green), 5 (light blue), 6 (dark blue), 7 (purple), and 8 (black) – are overlaid with the voltammogram obtained in the absence of acid (grey). **(B)** Stationary voltammograms of 0.5 mM $Co(dmgBF_2)_2(CH_3CN)_2$ in the presence of 5 mM 4-trifluoromethoxyanilinium collected using a working electrode subjected to stationary multiple cycling experiments (blue) has a $\Delta E_p[Co^{III/II}]$ that is 35 mV larger than that observed in voltammograms of the same solution collected with a freshly polished working electrode (red). The magnitude of this increase in peak-to-peak separation is far smaller than that observed in catalytic voltammograms collected with a working electrode previously subjected to analogous multiple cycling experiments collected under hydrodynamic conditions (grey). Voltammograms recorded at 0.1 V s^{-1} in 0.25 M $[NBu_4][PF_6]$ acetonitrile using a decamethylferrocene (0.25 mM) internal standard us a 5 mm OD glassy carbon working electrode.

SI-6 Electrochemical reduction of acids by glassy carbon

4-trifluoromethoxyanilinium

Variable rotation rate studies were recorded in a solution of 1.25 mM 4-trifluoromethoxyanilinium with 0.5 mM ferrocene. After each RDE voltammogram, the rotator was set to 0 rad sec^{-1} and a stationary voltammogram was collected. For both stationary and RDE measurements, a three-segment potential range that included the $Fc^{+/0}$ couple was used: the potential was first swept from -0.45 V to -1.23 V, then from -1.23 V to 0.3 V, and finally from 0.3 V back to -0.45 V. Because this potential range included the $Fc^{+/0}$ couple, the increase in baseline current observed during RDE measurements is attributed to the accumulation of the oxidized internal standard ferrocenium in solution.

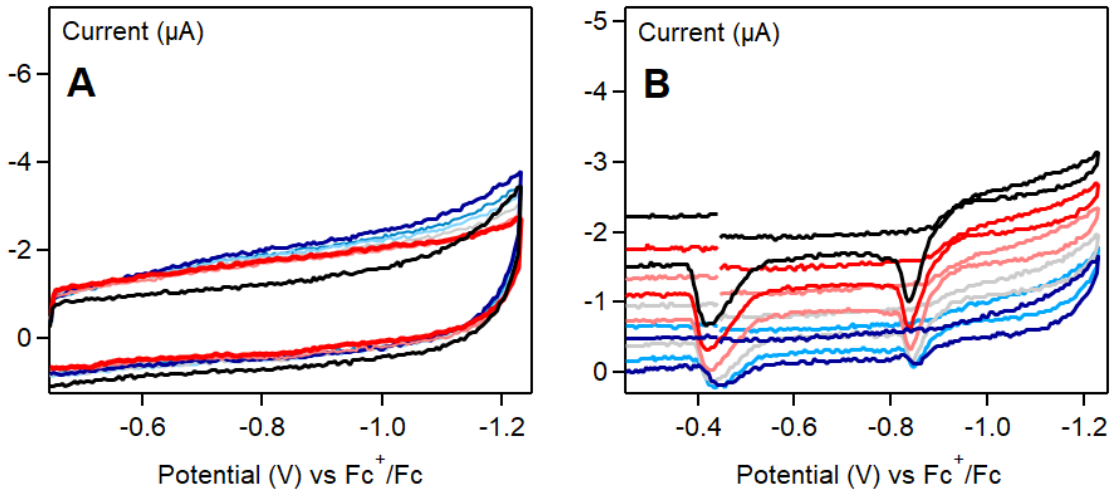

Figure S36 (A) Stationary voltammograms of 1.25 mM 4-trifluoromethoxyanilinium with 0.5 mM ferrocene in 0.25 M $[NBu_4][PF_6]$ acetonitrile collected before variable rotation rate study (black) and after RDE voltammograms at 42 (dark blue), 94 (blue), 168 (light blue), 262 (grey), 317 (pink), and 377 (red) rad sec^{-1}. Voltammograms recorded at 0.1 V s^{-1}. **(B)** Corresponding RDE voltammograms recorded at 0.01 V s^{-1} using rotation rates of 42 (dark blue), 94 (light blue), 168 (grey), 262 (pink), 317 (red), and 377 (black) rad sec^{-1}. Rotation rates varied in ascending order.

4-methoxyanilinium

Variable rotation rate studies were recorded in a solution of 1.25 mM 4-methoxyanilinium with 0.5 mM ferrocene. After each RDE voltammogram, the rotator was set to 0 rad sec^{-1} and a stationary voltammogram was collected. While the potential range employed during stationary measurements (-0.5 V to -1.3 V to 0.25 V to -0.5 V) included the $Fc^{+/0}$ redox couple, the potential range used during RDE

measurements (-0.5 V to -1.2 V to -0.46 V to -0.5 V) did not. The RDE voltammograms were referenced to the value of the $Fc^{+/0}$ couple observed in stationary measurements, which was constant across all stationary trials.

The $Fc^{+/0}$ redox couple was not included in the potential sweep during RDE measurements to avoid accumulation of ferrocenium in solution. No increase in baseline current was observed during these RDE measurements, unlike similar studies conducted with 4-trifluoromethoxyanilinium and trichloroacetic acid where the redox couple for the internal standard was traversed and an increase in baseline was observed.

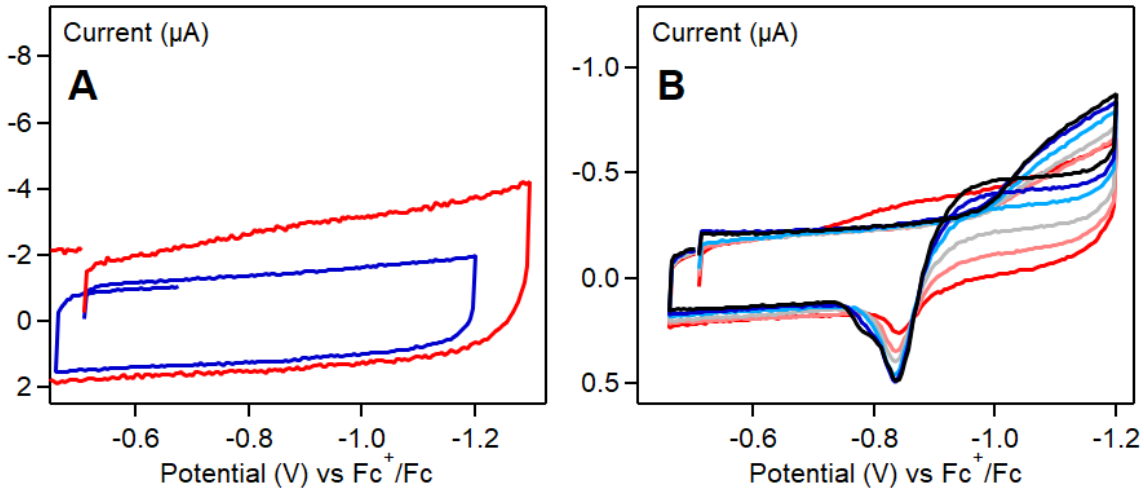

Figure S37 (A) Stationary voltammograms of 1.25 mM 4-methoxyanilinium with 0.5 mM ferrocene before (red) and after (blue) variable rotation rate studies. Voltammograms obtained in 0.25 M $[NBu_4][PF_6]$ acetonitrile at 0.1 V s^{-1}. **(B)** Corresponding RDE voltammograms at 42 (red), 94 (pink), 168 (grey), 262 (light blue), 317 (dark blue), and 377 (black) rad sec^{-1}. Rotation rates varied in ascending orders and voltammograms recorded 0.01 V s^{-1}.

Trichloroacetic acid

Variable rotation rate studies were recorded in a solution of 1.25 mM 4-trichloroacetic acid with 0.5 mM ferrocene. After each RDE voltammogram, the rotator was set to 0 rad sec^{-1} and a stationary voltammogram was collected. For both stationary and RDE measurements, a three-segment potential range that included the $Fc^{+/0}$ couple was used: the potential was first swept from -0.45 V to -1.2 V, then from -1.2 V to 0.3 V, and finally from 0.3 V back to -0.45 V. Because this potential range included the

$Fc^{+/0}$ couple, the increase in baseline current observed during RDE measurements is attributed to the accumulation of the oxidized internal standard ferrocenium in solution.

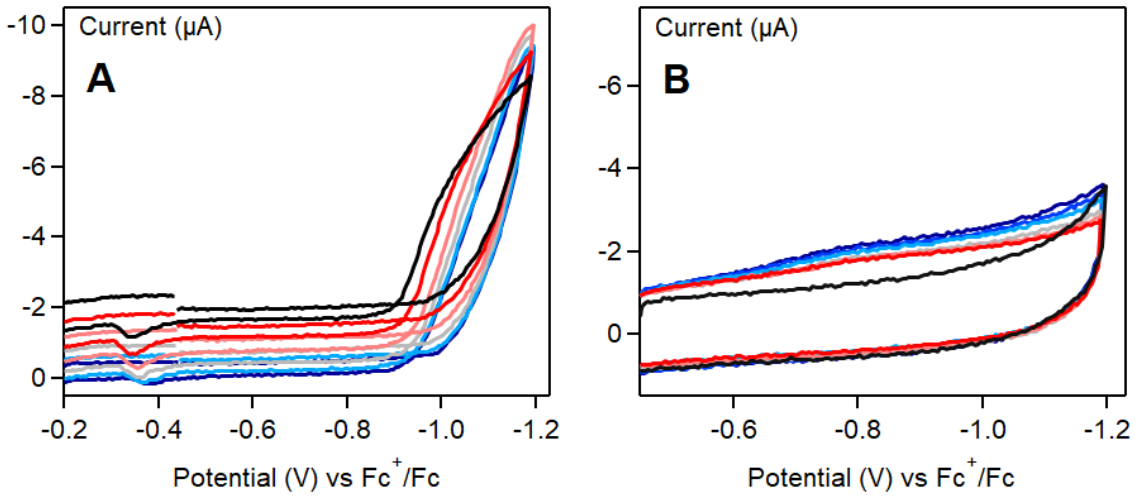

Figure S38 (A) RDE voltammograms of 1.25 mM trichloroacetic acid with 0.5 mM ferrocene in 0.25 M $[NBu_4][PF_6]$ acetonitrile at 0.01 V s^{-1}. Rotation rates varied in ascending order across the following range: 42 (dark blue), 94 (light blue), 168 (grey), 262 (pink), 317 (red), and 377 (black) rad sec^{-1}. **(B)** Stationary voltammograms collected before variable rotation rate study (black) and after RDE voltammograms at 42 (dark blue), 94 (blue), 168 (light blue), 262 (grey), 317 (pink), and 377 (red) rad sec^{-1}.

References

(1) Bard, A. J.; Faulkner, L. R. *Electrochemical Methods: Fundamentals and Applications*, 2nd ed.; Harris, D., Swain, E., Robey, C., Aiello, E., Eds.; John Wiley & Sons, Inc.: Hoboken, NJ, USA, 2001.

(2) Rountree, E. S.; Martin, D. J.; McCarthy, B. D.; Dempsey, J. L. Linear Free Energy Relationships in the Hydrogen Evolution Reaction: Kinetic Analysis of a Cobaloxime Catalyst. *ACS Catal.* **2016**, *6* (5), 3326–3335.

(3) Hu, X.; Brunschwig, B. S.; Peters, J. C. Electrocatalytic Hydrogen Evolution at Low Overpotentials by Cobalt Macrocyclic Glyoxime and Tetraimine Complexes. *J. Am. Chem. Soc.* **2007**, *129* (29), 8988–8998.

(4) Savéant, J.-M. *Elements of Molecular and Biomolecular Electrochemistry*; John Wiley & Sons, Inc.: Hoboken, NJ, USA, 2006.

(5) Costentin, C.; Savéant, J.-M. Multielectron, Multistep Molecular Catalysis of Electrochemical Reactions: Benchmarking of Homogeneous Catalysts. *ChemElectroChem* **2014**, *1* (7), 1226–1236.

(6) Wang, V. C.-C.; Johnson, B. A. Interpreting the Electrocatalytic Voltammetry of Homogeneous Catalysts by the Foot of the Wave Analysis and Its Wider Implications. *ACS Catal.* **2019**, *9* (8), 7109–7123.

(7) Muckerman, J. T.; Fujita, E. Theoretical Studies of the Mechanism of Catalytic Hydrogen Production by a Cobaloxime. *Chem. Commun.* **2011**, *47* (46), 12456-12458.

(8) Solis, B. H.; Hammes-Schiffer, S. Theoretical Analysis of Mechanistic Pathways for Hydrogen Evolution Catalyzed by Cobaloximes. *Inorg. Chem.* **2011**, *50* (21), 11252–11262.